

Pb Substitution with La Effect on the Magnetic, and Magnetocaloric Properties of $\text{La}_{1.995}\text{Pb}_{0.005}\text{NiMnO}_6$ Double Perovskite System

Arda Kandemir^{1, #} 

Increasing energy demands and growing environmental concerns, particularly regarding greenhouse gas emissions, make the development of sustainable technological alternatives necessary. Green technologies, such as the magnetocaloric cooling system based on the magnetocaloric effect, are promising solutions to these challenges. Therefore, it has gathered significant attention from scientists and research groups as a strong candidate to replace conventional cooling systems, offering enhanced effectiveness, greener technology, and lower production costs. For these purposes, $\text{La}_{1.995}\text{Pb}_{0.005}\text{NiMnO}_6$ double perovskite was synthesized by the sol-gel route. The crystal structure was characterized by X-ray Diffraction (XRD) at room temperature. Elemental distribution and surface morphology were investigated using Energy-Dispersive X-ray Spectroscopy (EDS) and Scanning Electron Microscopy (SEM), respectively. Another important property is the magnetic behavior of the compound therefore temperature and magnetic field-dependent magnetization ($M(T)$ and $M(H)$) analysis were investigated. From the investigation of the temperature dependence magnetization, there was a magnetic phase transition that occurred from the ferromagnetic to the paramagnetic phase near 213.34 K. Under 5T magnetic field variation, the maximum magnetic entropy change ($-\Delta S_M$) was determined and it is $0.23 \text{ Jkg}^{-1}\text{K}^{-1}$. According to the results, the compound that was investigated can be a candidate for use as a magnetic refrigerant in a low-temperature region. For making a valid magnetic cooling system that operates around room temperature, optimization studies are essential to be conducted.

1. Introduction

In the light of technological developments, there are regions that stay in the shadow of energy needs. Energy consumption rates increase year by year with technological leaps and population. However, this is not the major problem. Climate change and ozone depletion, on the other hand, threatened our lives and health. To enhance living standards sustainably, adjustments to current technologies are required. Green technologies can be a good candidate for what we are looking for. For instance, the cooling systems hold nearly 15% [1] of global energy usage. One of the cooling technologies is gas compression cooling system which is approaching their efficiency limits in terms of efficiency, and they are responsible for ozone depletion and global warming [2] due to the hydrofluorocarbons (HFCs), hydrochlorofluorocarbons (HCFCs) and chlorofluorocarbons (CFCs) leakage from system. Moreover, the production costs for current

technology are high [3, 4]. In contrast to conventional cooling technology, the magnetocaloric refrigeration systems are becoming a good candidate for a replacement as they are more effective, low in production cost, and green technology [4-11].

The magnetocaloric refrigeration system is based on magnetocaloric effect which can be described as a thermal answer while the magnetic sample is exposed to external magnetic field. MCE is related to change in total magnetic entropy or temperature change under adiabatic conditions [5, 11, 12]. The variation in alignment of magnetic moments, $-\Delta S_M^{max}$, occurs around the Curie temperature where magnetic material does a magnetic phase transition. These factors describe the performance of magnetic cooling refrigerants. Scientists have studied optimization of magnetic material to produce a practical magnetic cooling application.

¹ Department of Physics, Faculty of Science and Letters, Çukurova University, 01330 Adana, Türkiye

#Corresponding author: ardakandemir88@gmail.com

Keywords: Magnetocaloric effect; Magnetic refrigeration system; Affordable and clean energy; Double perovskite

Received: 20 April 2025 | Accepted: 10 June 2025 | Published online: 26 June 2025

J.NanoSci.Adv.Mater. 2025, 4 (1), 24

One of them is finding the required temperature value where the material does a phase transition from FM to PM phase. Another optimization study is achieving a high $-\Delta S_M^{max}$ value on that required temperature. For these objectives some studies were carried out on new compound families [6, 7, 9, 13-15]. In MC systems, Gadolinium (Gd) and gadolinium included alloys and compounds are the top classes [16] due to their MCE performance. In addition to these materials, Ni-Mn-Sn, Mn-As, La-Fe-Si, and Mn-P compounds are also valid material groups due to their MCE performance. However, their toxicity, irreversible cooling cycle and high-cost [17-19] push scientists to seek for new compound classes. According to this perspective, manganite perovskites represent a promising material family as they are chemically stable, exhibit a reversible cooling cycle, and are lower in cost over intermetallic alloys. [7, 9, 13, 20-25]. These features make manganite perovskite a possible magnetic cooling application.

The structural diversity in the manganite perovskite family due to the versatility of the elements from the periodic table can alter the physical features. The chemical representation of manganite perovskites is $R_{1-x}A_xMnO_3$ (R = rare earth, and A = alkaline earth). Furthermore, double perovskite manganite structure is a new chapter in the literature. Their formula can be denoted as $R_xA_{1-x}B_{1-x}TM_2O_6$ (R = rare earth, A&B = alkaline earth, and TM = Transition Metal). The notable low-temperature cooling performance of this material family makes scientists interested in further studies into this material structure. [26-28].

Furthermore, La_2NiMnO_6 is an example that is one of a rare-earth based double perovskite manganite, and it is a significant and multifunctional material due to its interesting structural and physical features [29-31]. The La_2NiMnO_6 sample was synthesized in different forms, such as single crystals, bulk polycrystals, nanoparticles, and thin films [29-31]. This La based material was studied according to different functional features such as magnetoresistance, magneto-capacitance, magneto-dielectric, and magnetocaloric features [29-31]. It is also used as a magnetic semiconductor and has become interested due to its potential in spintronic devices, such as magnetic memories and magnetodielectric capacitors [32].

Improving the magnetic phase transition temperature in this new perovskite manganite family may allow their use in practical cooling technologies. The studies with Pb substitution in the A-site of the perovskite structure from the literature show that it enhances the magnetic phase transition temperature that occurs around room temperature [33, 34].

Under these circumstances, the effects of Pb substitution on the magnetic and magnetocaloric features of $La_{1.995}Pb_{0.005}NiMnO_6$ were investigated.

2. Results and Discussion

The XRD patterns of the compound were recorded at room temperature, and it is given in Figure 1. The crystallographic structure refined by using the Rietveld's refinement method [35] in the Fullprof software [36] and the structural parameters that refined are summarized in Table 1. The graph of XRD points out that the sample successfully crystallized. The compound crystals in a rhombohedral structure (space group $R\bar{3}c$). Experimental results and the theoretical model used in the Rietveld refinement method are well matched, which can be seen from the convergence factor (χ^2) value. For the formation of the crystal structure, the average ionic radius of the A-site ($\langle r_A \rangle$) is an important parameter which can be calculated by arithmetic mean of the A-site ions' ionic radius. This parameter affects the distortion level of the perovskite structure.

The Goldschmidt tolerance factor is a parameter that points out the change in the A and B site of the crystal structure according to ions that are used and ionic radius of them. To determine the tolerance factor, the provided equation down below is used:

$$t_G = \frac{\langle r_A \rangle + r_O}{\sqrt{2}(\langle r_B \rangle + r_O)} = 1 \text{ (ideal structure)} \quad (1)$$

where $\langle r_A \rangle$, r_O , and r_B are the notations of the average A-site ionic radius, the ionic radius of oxygen ion, and the ionic radius of Mn and Ni ion, respectively. For the ionic radius value of Ni^{3+} , the low spin value was chosen from the effective ionic radius table [37]. From Table 1, the tolerance factor value is close to 1.00. This means the perovskite crystal structure for this compound is around the level of the ideal crystal structure. As there is a gap between the ideal and the crystal structure of the compound that is studied, it may be concluded that there is a distortion in the crystal structure. This distortion is notable because even small deviations from an ideal cubic structure can influence bond lengths and angles, thereby affecting electron hopping and eventually adjusting the material's electronic and magnetic features.

Besides the distortion level, the size mismatch effect coefficient (σ^2) is another factor which is important for the crystal structure. It indicates the dislocation in the A-site, and it can be calculated by using the equation below:

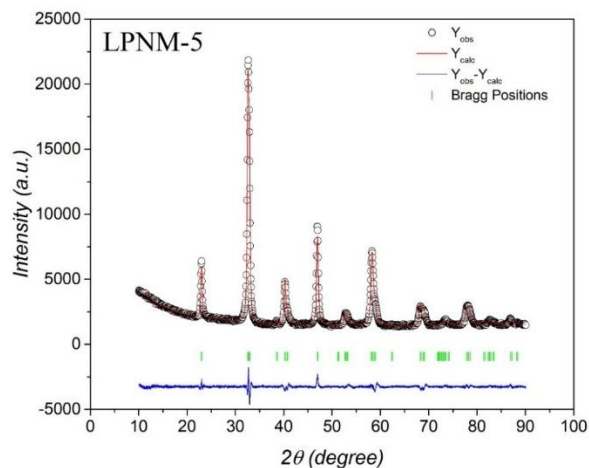


Figure 1. XRD Patterns of LPNM-5. The black circle, red line, blue line, and green bars represent the observed data, calculated data, differences between observed and calculated data, and Bragg positions respectively.

$$\sigma^2 = \sum_i x_i r_i^2 - \langle r_A \rangle^2 \quad (2)$$

where x_i , r_i , and $\langle r_A \rangle$ are the notations of the fractional occupancy of the i^{th} ion in the A-site, the ionic radii of the corresponding ion in the A-site, and the average ionic radius of the A-site, respectively. This value shows the degree of disorder in the A-site which can impact the bond angle and bond length of the compound. A change in these parameters can also affect electron scattering. The less electron scattering occurs due to lower value of σ^2 in the crystal structure. The less electron scattering can enhance the sample's electronic features and the conduction [38, 39].

In addition to structural parameters, the crystallite size (D) is another parameter which can affect the magnetic features and can be determined by the Debye-Scherrer equation [40, 41]:

$$D = \frac{\kappa\lambda}{\beta\cos\theta} \quad (3)$$

where κ , λ , and β denotes the crystallite shape factor (0.94 for each sample), the wavelength of the X-ray ($\lambda_{\text{Cu-K}\alpha} = 1.5406 \text{ \AA}$), and the peak full width at half maximum at the observed peak angle θ (in radians), respectively.

It is notable that the role of the e_g electron bandwidth (W) is also important for understanding the electronic and magnetic features of the substituted manganites. The equation for W is:

$$W = \cos \frac{\left(\frac{1}{2} [\pi - \langle \theta_{\text{Ni/Mn-O-Ni/Mn}} \rangle] \right)}{\langle R_{\text{Ni/Mn-O}} \rangle^{3.5}} \quad (4)$$

where the θ and R denotes the bond angle and bond length, respectively. In magnetic materials, the W value has an impact on metallic and ferromagnetism performance. The higher value of W is associated with higher Curie temperature, metal-insulator transition temperatures, and lower resistivity (ρ). The e_g electron bandwidth and t parameter which is a measure of the inter-site hopping interaction of e_g electrons, are directly proportional to each other. The movement of the d electrons between neighboring B-sites is responsible for this phenomenon. This phenomenon occurs due to the d electrons' motion among neighbor ions in the B-site. The motion of d electrons is known as super-transfer and it occurs through the oxygen (O) 2p orbitals [42]. Comparing the current compound with our previous studies from Table 1, the LPNM-5 compound has slightly broader W due to the larger average bond angle and shorter average bond length according to Equation (4). In the light of these changes, it results in a broader bandwidth which can affect the magnetic nature of the compound such as double-exchange mechanism.

According to Table 1, the volume parameter values of each sample with Pb are greater than the parent compound and this implies that the distortion occurred. Due to this distortion, the bond angle and the bond length of the samples with Pb content affected and larger than the parent compound's values which can impact the T_c values of the compounds.

Besides the structural features of the compound, morphological properties and elemental abundance were also conducted by using SEM and EDS analysis. These analysis illustrations were united and shown in Figure 2. From SEM images of the sample, the grain boundaries are noticeable and the presence of liquid phase [43] can induce grain agglomeration which can affect the physical characteristics of the sample, especially the magnetic behavior. The shape of grains is different sized polygonal with a high degree of homogeneity. The EDS analysis indicates that the stoichiometry of the compound is persevered during the sample preparation and heat treatment. EDS spectrum has only La, Pb, Ni, Mn, and O elements' signals that points out there is no contamination. Considering EDS results, the sample production of the perovskite successfully achieved avoiding any contamination or elemental ratio change.

From the SEM micrograph, the size of the grains was found using ImageJ software. For this process, one hundred grains were chosen randomly with observable boundaries. The bar chart of the grain size distribution of the sample is given in the inset of Figure 2. The mean value of the grain size is $0.42 \mu\text{m}$ for the compound according to the bar chart.

The magnetic and magnetocaloric characteristics of a compound are major components of the crystal structure as well as structural and morphological aspects. The temperature dependent magnetization $M(T)$ and inverse susceptibility graphs are combined with dual y-axis and given in Figure 3. The magnetization curve values are given on the left y-axis while the inverse susceptibility values are given on the right y-axis. Moreover, the temperature dependence of derivatives of the magnetization ($dM/dT - T$) of the compound is given inset of Figure 3. The $M(T)$ values measured under 250 Oe external magnetic field in both zero-field-cooled (ZFC) and field-cooled (FC) modes. The reduction in magnetization with respect to temperature rise represents a phase transition from ferromagnetism to paramagnetism. The bifurcation point, where FC and ZFC curves diverge indicates the magnetic phase transition temperature known as the Curie temperature. Furthermore, derivatives of magnetization with respect to temperature show the magnetic phase transition temperature in the inset of Figure 3 and the value of the Curie temperature (T_C) is given in Table 2. Below T_C , the compound displays irreversible magnetic behavior between ZFC and FC modes. It can be defined by several factors such as magnetic anisotropy, domain wall pinning effect, canted spins [44-47]. The gap between FC and ZFC cusps is in the low temperature region can be linked to the blocking temperature which indicate the presence of spin-cluster and metastable or spin-glass-like states [48, 49]. Above T_C region, the graph of the inverse susceptibility diverges from the fitted line which is known as the Curie-Weiss law. It is given in Figure 3 as a red arrow. The reason behind the divergence can be related to the Griffiths phase [50]. The change of a ferromagnet with the lack of magnetic ions which are in a magnetically ordered state can appear at a temperature that is lower than the ideal system. In this case, the Griffiths phase appears due to the ferromagnetic clusters in the paramagnetic matrix [51]. It is consistent with in the literature on disordered magnetic systems for the double perovskite structures [52]. The Curie-Weiss law is related with susceptibility and the temperature in the compound and the relation can be given as:

$$\chi = \frac{C}{T - \theta} \quad (5)$$

where C , and θ denote the Curie constant and the paramagnetic curie temperature, respectively. The mathematical formula of the C value can be calculated by:

$$C = \frac{N\mu_{eff}^2\mu_B^2}{3k} \quad (6)$$

where N , μ_{eff} , μ_B , and k_B denote, Avogadro's number, the effective magnetic moment, the Bohr magneton, and Boltzmann constant, respectively. Using the slope of the temperature dependent inverse susceptibility graph in the Curie-Weiss Law, the μ_{eff} parameter was determined and tabulated in Table 2 [22, 53].

The effective magnetic moment value of the LPNM-5 is lower than the LPNM-001 ($\text{La}_{1.99}\text{Pb}_{0.01}\text{NiMnO}_6$) sample but larger than the parent compound according to our previous studies. The gap between the two samples can be expressed as the super exchange mechanism is more dominant in the LPNM-5 sample, raising its antiferromagnetic feature. As the double exchange mechanism is less dominant, it affects the ferromagnetic nature of the sample and causes a reduction in the Curie temperature and magnetic entropy change value, which can be seen in Table 2. From this perspective, it also shows how the substitution amount impacts on the sample's magnetic nature.

The spontaneous magnetization of a sample is a result of the external magnetic field. In the isothermal magnetization analysis, the sample was exposed to varying external magnetic fields which were from 0-5 T during the magnetic phase transition temperature region for understanding how it affects. The spontaneous magnetization is given in Figure 4. Between each consecutive isothermal curve in $M(H)$ graph is a 4 K temperature gap. According to the $M(H)$ graph, magnetization is rising rapidly with respect to a small applied magnetic field at low temperature region. With increasing applied magnetic field, the magnetization exhibits an increment, yet it doesn't reach saturation. The short-range FM interactions, nonuniform magnetic properties, and the appearance of the FM clusters in the compound might restrict saturation [54]. Above T_C , the magnetization curves become almost linear which means that the paramagnetism feature of the compound is established by the random alignment of the magnetic moments because of thermal energy. According to these features, the compound undergoes a magnetic phase transition from the FM to PM phase.

In addition to $M(T)$ and $M(H)$ analysis, the magnetic entropy change ($-\Delta S_M$) is another major aspect that demonstrates the alteration in disorder in the orientation of magnetic moments. For determining magnetic entropy change, following equation was used:

$$-\Delta S_M = \Delta S_M(T, H) - \Delta S_M(T, 0) = \int_0^H \left(\frac{\partial S}{\partial H}\right)_T dH \quad (7)$$

and using Maxwell's thermodynamic relation,

$$\left(\frac{\partial M}{\partial T}\right)_H = \left(\frac{\partial S}{\partial H}\right)_T \quad (8)$$

the equation can be expressed as:

$$-\Delta S_M = \int_0^H \left(\frac{\partial M}{\partial T}\right)_H dT \quad (9)$$

As the data from the study is discrete, the integral calculation can be employed for (9):

$$-\Delta S_M = \sum_i \frac{M_i - M_{i+1}}{T_{i+1} - T_i} \Delta H_i \quad (10)$$

Using these equations to obtain $-\Delta S_M(T)$ values, the area under consecutive isothermal magnetization curves in $M(H)$ was calculated and illustrated in Figure 5. The maximum magnetic entropy change value is obtained from Figure 5 and given in Table 2. There are factors affecting to obtain $-\Delta S_M$ value of a compound [21]. One parameter is how the magnetic moments align in the sample. Another one is the double exchange interaction that is important for the ferromagnetic properties of a material. The double exchange interaction strongly impacts the orientation of magnetic moments in the sample.

Another important parameter affecting the magnetocaloric effect of a material is the relative cooling power (RCP). It can be obtained from $-\Delta S_M(T)$ curves by using the equation below:

$$RCP = -\Delta S_M^{max} \times \delta T_{FWHM} \quad (11)$$

where δT_{FWHM} denotes the full width at the half maximum of the $-\Delta S_M(T)$ curve. The RCP shows the material's ability to transfer heat between hot and cold reservoirs in the ideal thermodynamic cycle of magnetocaloric applications. As the $-\Delta S_M$ graph couldn't achieve Gaussian distribution, the value of the RCP couldn't be determined for this study and for this reason the value of RCP is tabulated as N/A in Table 2. The necessary temperature values fall outside the range of the PPMS equipment.

The magnetic phase transition order is another key aspect when it comes to deciding the proper material for magnetic refrigeration application. The materials exhibit first-order magnetic phase transition have high thermal and magnetic hysteresis which are unwanted properties. The compounds with a second-order magnetic phase transition on the other hand, have a smaller

hysteresis and that is why they are considered as candidates to be a refrigerant in magnetic refrigeration technology. To classify the order of the magnetic phase transition, the Banerjee's criterion [55] was applied to Arrott graph which is given in Figure 6. According to criteria, the negative slope of curves represents the material has a first-order magnetic phase transition whereas the positive slope of curves denotes the material has a first-order magnetic phase transition. The sample undergoes a second-order magnetic phase transition due to the positive slope of curves. This feature of the compound is associated with a reversible MCE that improves the compound practical usage.

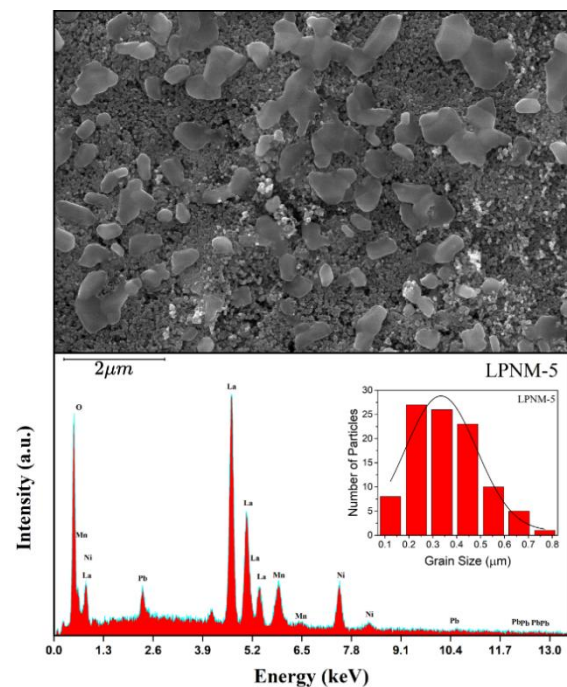


Figure 2. Analysis of SEM, EDS, and Grain Size Distribution for LPNM-5.

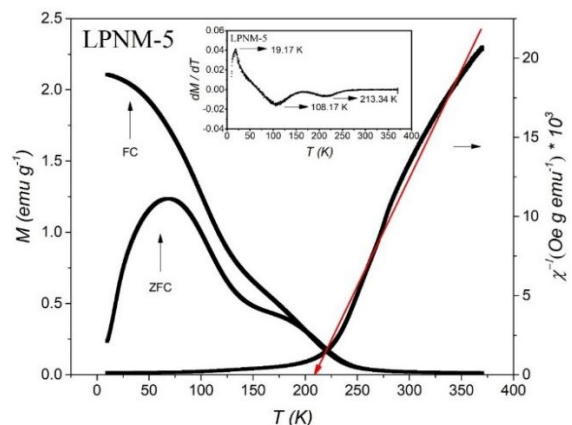


Figure 3. The magnetization measurement with FC and ZFC modes and the inverse susceptibility determined with respect to the temperature for LPNM-5.

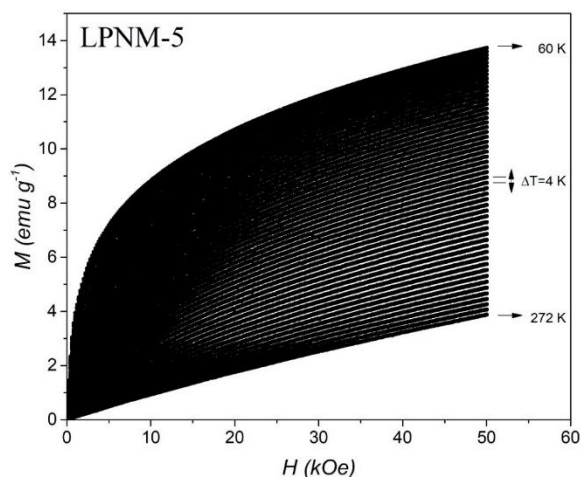


Figure 4. Applied magnetic field dependence of the magnetization curves measured at various temperatures near critical point (T_c) in steps of 4 K for LPNM-5.

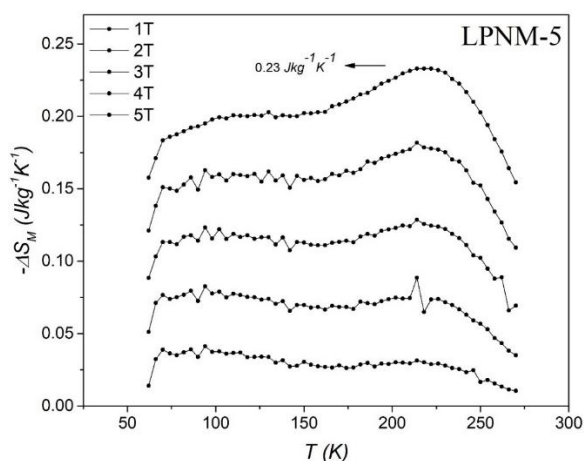


Figure 5. The magnetic entropy change with temperature ($-\Delta S_M(T)$) for LPNM-5.

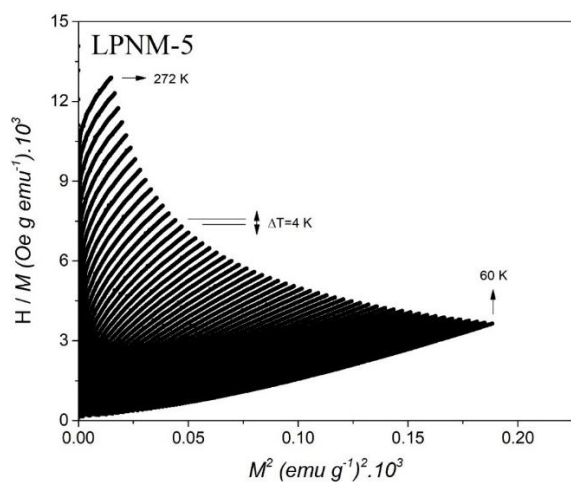


Figure 6. Arrott graph for LPNM-5.

3. Conclusion

The magnetic and magnetocaloric features of $\text{La}_{1.995}\text{Pb}_{0.005}\text{NiMnO}_6$ were investigated in terms of Pb substitution. To produce the sample the sol-gel technique was used.

XRD analysis results show that the compound's crystal structure is rhombohedral with the $R\bar{3}c$ space group.

According to $M(T)$ and $M(H)$ magnetic measurements, the sample undergoes a magnetic phase transition from FM to PM. The Curie temperature values were observed at 213.34 K from $M(T)$ analysis. The magnetic entropy change was calculated using the isothermal magnetization curves and it was found as $0.23 \text{ Jkg}^{-1}\text{K}^{-1}$ under the 5 T external magnetic field. Furthermore, the order of magnetic phase transition from FM to PM was the second order that was achieved from the Arrott graph.

From these aspects, the investigated compound is appropriate for magnetic refrigeration systems which operate at low temperature levels. While this material shows potential for the low-temperature region, the trend of magnetocaloric technology suggests the development of materials suitable for room-temperature applications. For that reason, further optimization studies are essential to advance the development of such materials for practical magnetic refrigeration systems. These optimization studies need to focus on tuning the magnetic entropy change and shifting the magnetic phase transition temperature would be required to potentially adapt such materials for practical magnetic cooling applications closer to the required conditions, thereby expanding their benefit.

Method

To achieve polycrystalline $\text{La}_{1.995}\text{Pb}_{0.005}\text{NiMnO}_6$ double perovskite manganite, the sol-gel production route was used. The compound was labeled as LPNM-5. With proper stoichiometric quantities of $\text{La}(\text{NO}_3)_3 \cdot 6\text{H}_2\text{O}$ (99.999% purity, Aldrich), $\text{Pb}(\text{NO}_3)_2$ ($\geq 99.5\%$ purity, Aldrich), $\text{Ni}(\text{NO}_3)_2 \cdot 6\text{H}_2\text{O}$ (99% purity, Merck) and $\text{Mn}(\text{NO}_3)_2 \cdot x\text{H}_2\text{O}$ (99.9% purity, Bostonchem) were used and mixed using appropriate pure water for each starting chemical content to achieve aqueous solutions. Next, they were mixed to have a single solution. Forming a sol-gel, the reagent and solvent chemicals selected as citric acid monohydrate (CAS Number: 5949-29-1, Aldrich) and ethylene glycol ($\geq 99\%$ purity, Aldrich), respectively. The total metal ions to citric acid molar ratio of 1:5 was used. The heating was kept constant at $300 \text{ }^\circ\text{C}$ while the stirring process continued to achieve a dry gel form. To remove

organic residues and promote the formation of metal oxides, the dried gel was combusted at 550 °C in air for an hour. The calcination process follows the burning process at 600°C for six hours in air with an 8°C per minute heating and cooling rates. To obtain uniform mixture, grinding and mixing process applied by using mortar grinder (Retsch RM 200) for ten minutes with 6 repeats. The resulting powder was then pressed into pellets by using a hydraulic press (Maassen MP 250) under 5 tons pressure. The last step of the sample production is sintering which was conducted in the air at 1000°C for 24 hours. The heating and cooling rates in the sintering were the same as the calcination process.

After all production steps were completed, the final compound was investigated in Çukurova University Central Research Laboratory (ÇÜMERLAB) for all measurements, analysis, and techniques. For characterization of the crystal structure and the phase purity of the compound, the X-ray diffraction (XRD) with CuK α radiation ($\lambda = 1.5406 \text{ \AA}$) conducted at room temperature. The 2θ range that was scanned in the XRD is between 10 and 90 degrees. For this scanning range, 2.5 degrees scanned per minute with a 0.013 step size.

The data collected from XRD analysis were investigated by using the X'Pert High Score Plus software, Fullprof fitting software, and the Rietveld refinement method.

To understand the morphological and elemental abundance of the compound, the Scanning Electron Microscope (SEM) analysis and Energy Dispersive X-Ray Spectroscopy (EDS) were performed, respectively.

To examine the magnetic nature of the compound such as temperature dependence $M(T)$ and field dependence $M(H)$ features, the Vibration Sample Magnetometer (VSM) equipped with a Physical Properties Measurement System (PPMS) was utilized. In $M(T)$ measurement zero-field-cooled (ZFC) and field-cooled (FC) modes were applied, and the operation temperature range of each mode was between 10 K to 350 K. In ZFC mode, the compound was cooled down to 10 K without any external magnetic field. After achieving the magnetic phase transition temperature from ferromagnetism to paramagnetism, the isothermal magnetization measurements conducted under varying external magnetic field from 0 to 5 T to determine the magnetic entropy change.

Table 1. The structural parameters of La₂NiMnO₆ [56], LPNM-5, and LPNM-001 [57] compounds. The lattice parameters of the structure (a, b, c, and unit cell volume (V)), the crystal structures with space groups, tolerance factor (t_f), average ionic radius of the A-site, average bond angle of Ni/Mn-O-Ni/Mn, average bond length of Ni/Mn-O, crystallite size (D), size mismatch effect coefficient (σ^2), the bandwidth (W), and convergence factor χ^2 values for the compounds.

Structural Parameters	La ₂ NiMnO ₆	LPNM-5	LPNM-001
a (Å)	5.4743	5.4932	5.49992
b (Å)	5.4743	5.4932	5.49992
c (Å)	13.2607	13.283	13.2417
V (Å ³)	344.1534	347.1184	346.8863
Crystal Structure	Rhombohedral	Rhombohedral	Rhombohedral
Space Group	$R\bar{3}c$	$R\bar{3}c$	$R\bar{3}c$
t_f	N/A	0.9947	1.0009
$\langle r_A \rangle$ (Å)	N/A	1.353	1.3425
$\langle \text{Ni/Mn-O-Ni/Mn} \rangle$ (°)	156.13	167.5173	160.7158
$\langle d_{\text{Ni/Mn-O}} \rangle$ (Å)	1.92861	1.9538	1.9582
D (nm)	21.74	15.6464	27.4326
σ^2 (Å ²)	N/A	0.000441	0.000919
W	N/A	0.095362	0.093831
χ^2	3.97	2.62	4.57
Reference	[56]	Current Work	[57]

Table 2. The magnetic and magnetocaloric parameters for La₂NiMnO₆ [56], LPNM-5, and LPNM-001 [57] compounds.

Sample	T _c (K)	μ _{eff} (mB)	-ΔS _M (J kg ⁻¹ K ⁻¹)	RCP (J kg ⁻¹)	Reference
La ₂ NiMnO ₆	200	1.75	0.21	46.2	[56]
LPNM-5	213.34	2.34	0.23	N/A	Current Work
LPNM-001	223.73	10.4	0.56	79.3	[57]

Authors' Contributions:

AK: Investigation, Resources, Data Curation, Formal analysis, Writing - Original Draft, Writing - Review & Editing.

Data Availability Statement

The data that support the findings of this study are available from the corresponding author upon reasonable request.

Declaration of Ethical Standards

The author(s) of this article declare that the materials and methods used in this study do not require ethical committee permission and/or legal-special permission.

Conflict of Interest

There is no conflict of interest in this study.

References

- [1] Tassou, S.A., Ge, Y., Hadaway, A., and Marriott, D., Energy consumption and conservation in food retailing. *Applied Thermal Engineering*, **31**(2), 147-156, (2011).
- [2] Eskandari, M.A., Brahiti, N., Hussain, I., Balli, M., and Fournier, P., Magnetic and magnetocaloric properties of Pr₂CuMnO₆. *Physica B: Condensed Matter*, **649**, 414397, (2023).
- [3] Gschneidner Jr, K.A., Pecharsky, V.K., Pecharsky, A.O., and Zimm, C.B., Recent Developments in Magnetic Refrigeration. *Materials Science Forum*, **315-317**, 69-76, (1999).
- [4] Ayaş, A.O., Akyol, M., and Ekicibil, A., Structural and magnetic properties with large reversible magnetocaloric effect in (La 1-x Pr x) 0.85 Ag 0.15 MnO 3 (0.0 ≤ x ≤ 0.5) compounds. *Philosophical Magazine*, **96**(10), 922-937, (2016).
- [5] Gschneidner, K.A. and Pecharsky, V.K., *Recent developments in magnetic refrigeration*. 209-221, (1996).
- [6] Gschneidner, K.A. and Pecharsky, V.K., Magnetocaloric Materials. *Annual Review of Materials Science*, **30**(1), 387-429, (2000).

[7] Phan, M.-H. and Yu, S.-C., Review of the magnetocaloric effect in manganite materials. *Journal of Magnetism and Magnetic Materials*, **308**(2), 325-340, (2007).

[8] Ayaş, A.O., Kılıç Çetin, S., Akyol, M., Akça, G., and Ekicibil, A., Effect of B site partial Ru substitution on structural magnetic and magnetocaloric properties in La_{0.7}Pb_{0.3}Mn_{1-x}Ru_xO₃ (x = 0.0, 0.1 and 0.2) perovskite system. *Journal of Molecular Structure*, **1200**, 127120-127120, (2020).

[9] Ayaş, A.O., Çetin, S.K., Akça, G., Akyol, M., and Ekicibil, A., Magnetic refrigeration: Current progress in magnetocaloric properties of perovskite manganite materials. *Materials Today Communications*, **35**, 105988, (2023).

[10] Kandemir, A., Akça, G., Kılıç Çetin, S., Ayaş, A.O., Akyol, M., and Ekicibil, A., Effects of Ca substitution on magnetic and magnetocaloric properties in PrBa_{1-x}CaxMn₂O₆ system. *Journal of Solid State Chemistry*, **324**, 124086, (2023).

[11] Gutfleisch, O., Willard, M.A., Brück, E., Chen, C.H., Sankar, S.G., and Liu, J.P., Magnetic Materials and Devices for the 21st Century: Stronger, Lighter, and More Energy Efficient. **23**(7), 821-842, (2011).

[12] Zhang, Y., Tian, Y., Zhang, Z., Jia, Y., Zhang, B., Jiang, M., Wang, J., and Ren, Z., Magnetic properties and giant cryogenic magnetocaloric effect in B-site ordered antiferromagnetic Gd₂MgTiO₆ double perovskite oxide. *Acta Materialia*, **226**, 117669, (2022).

[13] Ram, N.R., Prakash, M., Naresh, U., Kumar, N.S., Sarmash, T.S., Subbarao, T., Kumar, R.J., Kumar, G.R., and Naidu, K.C.B., Review on Magnetocaloric Effect and Materials. *Journal of Superconductivity and Novel Magnetism*, **31**(7), 1971-1979, (2018).

[14] Franco, V., Blázquez, J.S., Ipus, J.J., Law, J.Y., Moreno-Ramírez, L.M., and Conde, A., Magnetocaloric effect: From materials research to refrigeration devices. *Progress in Materials Science*, **93**, 112-232, (2018).

[15] Lyubina, J., Magnetocaloric materials for energy efficient cooling. *Journal of Physics D: Applied Physics*, **50**(5), 53002-53002, (2017).

[16] Pecharsky, V.K. and Gschneidner K. A, Jr., Giant Magnetocaloric Effect in Gd₅(Si₂Ge₂). *Physical Review Letters*, **78**(23), 4494-4497, (1997).

[17] Kim, Y.K. and Cho, Y.W., Magnetic transition of (MnFe)_yP_{1-x}As_x prepared by mechanochemical reaction and post-annealing. *Journal of Alloys and Compounds*, **394**(1-2), 19-23, (2005).

[18] Shah, I.A., ul Hassan, N., keremu, A., Riaz, S., Naseem, S., Xu, F., and Ullah, Z., Realization of Magnetostructural Transition and Magnetocaloric Properties of Ni-Mn-Mo-Sn Heusler Alloys.

Journal of Superconductivity and Novel Magnetism, **32**(3), 659-665, (2018).

[19] Lyubina, J., Schafer, R., Martin, N., Schultz, L., and Gutfleisch, O., Novel design of La(Fe,Si)₁₃ alloys towards high magnetic refrigeration performance. *Adv Mater*, **22**(33), 3735-3739, (2010).

[20] Barman, A., Kar-Narayan, S., and Mukherjee, D., Caloric Effects in Perovskite Oxides. *Advanced Materials Interfaces*, **6**(15), 1900291-1900291, (2019).

[21] Zhong, W., Au, C.-T., and Du, Y.-W., Review of magnetocaloric effect in perovskite-type oxides. *Chinese Physics B*, **22**(5), 57501-57501, (2013).

[22] Srivastava, S.K., Samantaray, B., Bora, T., and Ravi, S., Magnetic and electrical properties of Mn-substituted (La_{0.85}Ag_{0.15})CoO₃ compounds. *Journal of Magnetism and Magnetic Materials*, **474**, 605-612, (2019).

[23] Srivastava, S.K. and Ravi, S., Magnetic properties of Nd_{1-x}Ag_xMnO₃ compounds. *Journal of Physics: Condensed Matter*, **20**(50), (2008).

[24] Srivastava, S.K., Kar, M., Ravi, S., Mishra, P.K., and Babu, P.D., Magnetic properties of electron-doped Y_{1-x}Ce_xMnO₃ compounds. *Journal of Magnetism and Magnetic Materials*, **320**(19), 2382-2386, (2008).

[25] Mohamed, Z., Tka, E., Dhahri, J., and Hlil, E.K., Giant magnetic entropy change in manganese perovskite La_{0.67}Sr_{0.16}Ca_{0.17}MnO₃ near room temperature. *Journal of Alloys and Compounds*, **615**, 290-297, (2014).

[26] Krishna Murthy, J., Devi Chandrasekhar, K., Mahana, S., Topwal, D., and Venimadhav, A., Giant magnetocaloric effect in Gd₂NiMnO₆ and Gd₂CoMnO₆ ferromagnetic insulators. *Journal of Physics D: Applied Physics*, **48**(35), 355001-355001, (2015).

[27] Moon, J.Y., Kim, M.K., Choi, Y.J., and Lee, N., Giant Anisotropic Magnetocaloric Effect in Double-perovskite Gd₂CoMnO₆ Single Crystals. *Scientific Reports*, **7**(1), 16099-16099, (2017).

[28] Moon, J.Y., Kim, M.K., Oh, D.G., Kim, J.H., Shin, H.J., Choi, Y.J., and Lee, N., Anisotropic magnetic properties and giant rotating magnetocaloric effect in double-perovskite Tb₂CoMnO₆. *Physical Review B*, **98**(17), 174424-174424, (2018).

[29] Vinod, K., Sathyanarayana, A.T., Nithya, R., Gangopadhyay, P., and Mani, A., Studies on magnetic and magnetocaloric properties of double perovskite $\text{La}_{1-x}\text{Ni}_x\text{MnO}_6$ system. *Indian Journal of Physics*, **98**(6), 2023-2030, (2024).

[30] Hossain, A., Atique Ullah, A.K.M., Sarathi Guin, P., and Roy, S., An overview of La₂NiMnO₆ double perovskites: synthesis, structure, properties, and applications. *Journal of Sol-Gel Science and Technology*, **93**(3), 479-494, (2020).

[31] Chen, X., Xu, J., Xu, Y., Luo, F., and Du, Y., Rare earth double perovskites: a fertile soil in the field of perovskite oxides. *Inorganic Chemistry Frontiers*, **6**(9), 2226-2238, (2019).

[32] Luo, X., Sun, Y.P., Wang, B., Zhu, X.B., Song, W.H., Yang, Z.R., and Dai, J.M., The magnetic entropy change in the double perovskite La₂NiMnO₆ with strong spin-phonon coupling. *Solid State Communications*, **149**(19), 810-813, (2009).

[33] Ho, T.A., Thanh, T.D., Thang, P.D., Lee, J.S., Phan, T.L., and Yu, S.C., Magnetic Properties and Magnetocaloric Effect in Pb-Doped La_{0.9}Dy_{0.1}MnO₃ Manganites. *IEEE Transactions on Magnetics*, **50**(6), 1-4, (2014).

[34] Ayaş, A.O., Structural and magnetic properties with reversible magnetocaloric effect in PrSr_{1-x}Pb_xMn₂O₆ (0.1 ≤ x ≤ 0.3) double perovskite manganite structures. *Philosophical Magazine*, **98**(30), 2782-2796, (2018).

[35] Rietveld, H., A profile refinement method for nuclear and magnetic structures. *Journal of Applied Crystallography*, **2**(2), 65-71, (1969).

[36] Rodríguez-Carvajal, J., Recent advances in magnetic structure determination by neutron powder diffraction. *Physica B: Condensed Matter*, **192**(1), 55-69, (1993).

[37] Shannon, R.D., Revised effective ionic radii and systematic studies of interatomic distances in halides and chalcogenides. *Acta Crystallographica Section A*, **32**(5), 751-767, (1976).

[38] Soylu Koc, N., Altintas, S.P., Mahamdioua, N., and Terzioglu, C., Cation size mismatch effect in (La_{1-y}RE_y)_{1.4}Ca_{1.6}Mn₂O₇ perovskite manganites. *Journal of Alloys and Compounds*, **797**, 471-476, (2019).

[39] Venkataiah, G., Prasad, V., and Venugopal Reddy, P., Influence of A-site cation mismatch on structural, magnetic and electrical properties of lanthanum manganites. *Journal of Alloys and Compounds*, **429**(1), 1-9, (2007).

[40] Debye, P. and Scherrer, P., Interference on inordinate orientated particles in roentgen light. *Physikalische Zeitschrift*, **17**, 277-283, (1916).

[41] Debye, P. and Scherrer, P., Interference on inordinate orientated particles in x-ray light. III. *Physikalische Zeitschrift*, **18**, 291-301, (1917).

[42] Tokura, Y., Critical features of colossal magnetoresistive manganites. *Reports on Progress in Physics*, **69**(3), 797-851, (2006).

[43] Koc, R. and Anderson, H.U., Liquid phase sintering of LaCrO₃. *Journal of the European Ceramic Society*, **9**(4), 285-292, (1992).

[44] Debnath, J.C., Zeng, R., Kim, J.H., Shamba, P., Chen, D.P., and Dou, S.X., Effect of frozen spin on the magnetocaloric property of La_{0.7}Ca_{0.3}CoO₃ polycrystalline and single crystal samples. *Journal of Alloys and Compounds*, **510**(1), 125-133, (2012).

[45] Kılıç Çetin, S., Acet, M., and Ekicibil, A., Effect of Pr-substitution on the structural, magnetic and magnetocaloric properties of (La_{1-x}Pr_x)_{0.67}Pb_{0.33}MnO₃ (0.0 ≤ x ≤ 0.3) manganites. *Journal of Alloys and Compounds*, **727**, 1253-1262, (2017).

[46] Taşarkuyu, E., Coşkun, A., Irmak, A.E., Aktürk, S., Ünlü, G., Samancıoğlu, Y., Yücel, A., Sarıkürkcü, C., Aksoy, S., and Acet, M., Effect of high temperature sintering on the structural and the magnetic properties of La_{1.4}Ca_{1.6}Mn₂O₇. *Journal of Alloys and Compounds*, **509**(9), 3717-3722, (2011).

[47] Yang, J., Song, W.H., Ma, Y.Q., Zhang, R.L., Zhao, B.C., Sheng, Z.G., Zheng, G.H., Dai, J.M., and Sun, Y.P., Structural, magnetic, and transport properties in the Pr-doped manganites La_{0.9-x}Pr_xTe_{0.1}MnO₃ (0 ≤ x ≤ 0.9). *Physical Review B*, **70**(14), 144421-144421, (2004).

[48] Rana, D.S., Kuberkar, D.G., and Malik, S.K., Field-induced abrupt change in magnetization of the manganite compounds (La_R)_{0.45}(CaSr)_{0.55}MnO₃ (R = Eu and Tb). *Physical Review B*, **73**(6), 064407, (2006).

[49] Bourouina, M., Krichene, A., Chniba Boudjada, N., and Boujelben, W., Structural disorder effect on the structural and

magnetic properties of $\text{Pr}_{0.4}\text{Re}_{0.1}\text{Sr}_{0.5-y}\text{Ba}_y\text{MnO}_3$ manganites (Re = Pr, Sm, Eu, Gd, Dy and Ho). **43**(15), 12311-12320, (2017).

[50] Phong, P.T., Manh, D.H., Hoan, L.C., Ngai, T.V., Phuc, N.X., and Lee, I.-J., Particle size effects on $\text{La}_{0.7}\text{Ca}_{0.3}\text{MnO}_3$: Griffiths phase-like behavior and magnetocaloric study. *Journal of Alloys and Compounds*, **662**, 557-565, (2016).

[51] Krivoruchko, V.N., The Griffiths phase and the metal-insulator transition in substituted manganites (Review Article). *Low Temperature Physics*, **40**(7), 586-599, (2014).

[52] Mandal, P.R. and Nath, T.K., Evolution of Griffith phase in hole doped double perovskite $\text{La}_{2-x}\text{Sr}_x\text{CoMnO}_6$ ($x= 0.0, 0.5, \text{ and } 1.0$). *Materials Research Express*, **2**(6), (2015).

[53] Mugiraneza, S. and Hallas, A.M., Tutorial: a beginner's guide to interpreting magnetic susceptibility data with the Curie-Weiss law. *Communications Physics*, **5**(1), 95, (2022).

[54] Phong, P.T., Dang, N.V., Bau, L.V., An, N.M., and Lee, I.-J., Landau mean-field analysis and estimation of the spontaneous magnetization from magnetic entropy change in $\text{La}_{0.7}\text{Sr}_{0.3}\text{MnO}_3$ and $\text{La}_{0.7}\text{Sr}_{0.3}\text{Mn}_{0.95}\text{Ti}_{0.05}\text{O}_3$. *Journal of Alloys and Compounds*, **698**(C), 451-459, (2017).

[55] Banerjee, B.K., On a generalised approach to first and second order magnetic transitions. *Physics Letters*, **12**(1), 16-17, (1964).

[56] Ayaş, A.O., Sever, İ.B., Kandemir, A., and Ekicibil, A., The Sintering Temperature Effect on Magnetocaloric Effect in $\text{La}_2\text{MnNiO}_6$ Double Perovskite Manganite Material. *Adiyaman University Journal of Science*, **13**(1&2), 28-42, (2023).

[57] Kandemir, A., Ayaş, A.O., and Ekicibil, A. *Impact of Pb on structural, magnetic, and magnetocaloric features in $\text{La}_{1.99}\text{Pb}_{0.01}\text{NiMnO}_6$ double perovskite manganite sample.* in *5th International Eurasian Conference on Science, Engineering and Technology (EurasianSciEnTech 2024)*. 2024. Ankara, Türkiye.